12-2012

Design of Broadband Highly Efficient Harmonic-Tuned Power Amplifier Using In-Band Continuous Class(-1)/F Mode Transferring

Kenle Chen
Birck Nanotechnology Center, Purdue University, chen314@purdue.edu

Dimitrios Peroulis
Birck Nanotechnology Center, Purdue University, dperouli@purdue.edu

Chen, Kenle and Peroulis, Dimitrios, "Design of Broadband Highly Efficient Harmonic-Tuned Power Amplifier Using In-Band Continuous Class(-1)/F Mode Transferring" (2012). *Birck and NCN Publications.* Paper 1092.
http://dx.doi.org/10.1109/TMTT.2012.2221142

Design of Broadband Highly Efficient Harmonic-Tuned Power Amplifier Using In-Band Continuous Class-F^{-1}/F Mode Transferring

Kenle Chen, *Student Member, IEEE*, and Dimitrios Peroulis, *Member, IEEE*

***Abstract*—A novel methodology for designing high-frequency broadband harmonic-tuned power amplifiers (PAs) is presented in this paper. Specifically, a hybrid PA mode, transferring between continuous inverse Class-F and continuous Class-F, is for the first time employed to design PAs with optimal performance over more than-an-octave bandwidth. A GaN PA is designed and realized based on this mode-transferring operation using a three-stage transmission-line-based low-pass matching network. Simulation and experimental results show that an in-band PA-mode transferring between continuous Class-F^{-1} and continuous Class-F is successfully performed. The implemented PA achieves a measured 87% bandwidth from 1.3 to 3.3 GHz, while exhibiting a state-of-the-art performance of >10-dB gain, 60%–84% efficiency, and 10-W output power throughout this band. Furthermore, modulated evaluation is carried out using a 300-kHz bandwidth 16-quadrature amplitude-modulation signal. Good linearity performance is measured with adjacent channel power ratio from −20 to −35 dBc and an error vector magnitude of 4%–9% over the entire bandwidth.**

***Index Terms*—Broadband, continuous Class-F, continuous inverse Class-F, efficiency, GaN, harmonic tuned, low-pass matching network (MN), mode transferring, power amplifier (PA), synthesis.**

I. Introduction

NEXT-GENERATION wireless communication systems are required to operate at different communication standards/frequency bands for different applications. An ever-increasing number of high-frequency bands are being included for achieving high data transmission ratios, such as long term evolution (LTE) and worldwide interoperability for microwave access (WiMax). Consequently, power amplifiers (PAs) need to operate efficiently over a broad frequency range often spanning octave-wide bandwidths. Class-E PA mode has been extensively utilized in designing and implementing broadband PAs [1]–[3] due to its fairly simple circuitry and high efficiency. However, such a switch-mode operation fails at high frequencies (see Class-E theoretical limitation [4], [5]), as its parallel capacitor cannot be fully charged or discharged to support the ideal drain waveforms, leading to an efficiency degradation [6].

Harmonic-tuned PA modes, including Class-F and inverse Class-F, have been the leading candidates for realizing high-efficiency PAs at higher frequencies. These PA modes require multiple accurate harmonic terminations to present to the transistor, enforcing nonoverlapped waveforms of drain voltage and current with either square or half-sinusoidal shapes. As a result, they usually have very narrow instantaneous bandwidths in their frequency responses. To extend the operational bandwidth, advanced harmonic-tuned PA modes have been proposed and recently demonstrated, known as Class-J [7], [8], continuous Class-F [9], [10], and continuous inverse Class-F [11], [12]. These extended PA modes alleviate the precise harmonic requirements of the standard ones by offering multiple impedance solutions that can be dynamically distributed over the desired bandwidth, while maintaining the expected output power and efficiency. The harmonic requirements can be further relieved by the nonlinear output capacitor of the transistor, which assists to shape the output voltage waveform [13]–[15].

To date, several broadband PAs have been developed using the continuous PA mode with very efficient performances [15], [16], i.e., >70% average efficiencies over >50% bandwidths. However, it is worth noting that these reported PAs are designed within fairly low-frequency bands with center frequencies lower than 2 GHz, and they operate in an approximated continuous Class-F mode due to the difficulty in controlling both second and third harmonics simultaneously across a substantial bandwidth. Higher frequency designs with ≥80% efficiency require optimally tuned second and third harmonic impedances besides the fundamental one [17], [18]. In turn, it is of great importance to find an approach to properly control the second and third harmonics for designing and realizing broadband harmonic-tuned PAs. To accomplish this, the selection of PA mode needs to be considered together with the matching network (MN) realizability.

In [19], we have proposed and experimentally demonstrated a broadband harmonic tuning method for PA design based on in-band mode transferring, which is developed from a dual-band PA design [20]. This paper significantly expands our previous work presented in [19]. First, the design concept is extended from mode transferring between Class-F and Class-F^{-1} to a more general case of continuous Class-F and continuous Class-F^{-1}. We also show that this generalization greatly enhances the broadband PA design space and underlines

Manuscript received July 10, 2012; revised September 21, 2012; accepted September 24, 2012. Date of publication October 22, 2012; date of current version December 13, 2012. This paper is an expanded paper from the IEEE MTT-S International Microwave Symposium, Montreal, QC, Canada, June 17–22, 2012.

The authors are with the School of Electrical and Computer Engineering and the Birck Nano Technology Center, Purdue University, West Lafayette, IN 47906 USA (e-mail: chen314@purdue.edu; dperouli@purdue.edu).

Color versions of one or more of the figures in this paper are available online at http://ieeexplore.ieee.org.

Digital Object Identifier 10.1109/TMTT.2012.2221142

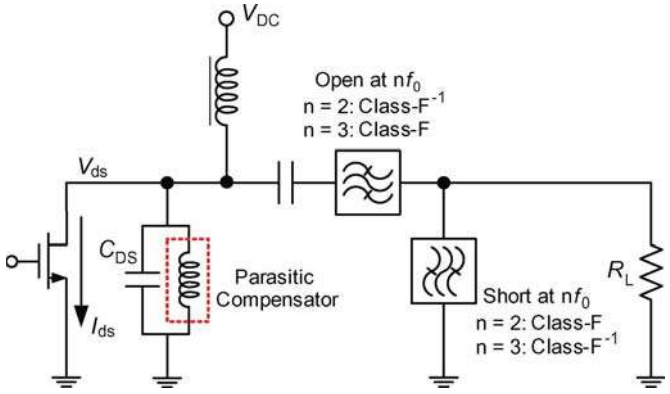

Fig. 1. Class-F and inverse Class-F PA topology with ideal second and third harmonic terminations.

that the design in [19] is a special case of the more general one presented here. Second, the PA design in [19] is further optimized achieving a higher measured efficiency over the entire frequency range, e.g., up to 5% improvement at the higher half band. Third, modulated-evaluation results are presented in this paper with a 0.3-MHz bandwidth quadrature-amplitude-modulation (QAM) modulated signal, showing a good potential of this PA for application in practical communication systems.

II. Harmonic-Tuned PA Theory

A. Standard Class-F/F^{-1} PA Modes

The standard Class-F PA is developed from the Class-B PA mode by loading the active device output with proper terminations at its fundamental and harmonic frequencies [21]. The half-sinusoidal current waveform, formed by the Class-B bias condition, has the following expression:

$$\begin{aligned} i_{\mathrm{F}}(\theta) &= I_{\mathrm{peak}}\cos\theta, \qquad -\pi/2 < \theta < \pi/2 \\ &= 0, \qquad -\pi < \theta \le -\pi/2; \quad \pi/2 \le \theta \le \pi \end{aligned} \tag{1}$$

The above equation (1) can be expressed using Fourier series (normalized to I_{peak}), given by [15]

$$i_{\mathrm{F}}(\theta) = \frac{1}{\pi} + \frac{1}{2}\cos\theta + \frac{2}{3\pi}\cos 2\theta - \frac{2}{15\pi}\cos 4\theta + \cdots. \tag{2}$$

The output MN (filter) is required to provide open-circuit (O.C.) terminations at odd harmonics and short-circuit (S.C.) terminations at even harmonics, as shown in Fig. 1. Thus, a square voltage waveform is shaped, which has no overlap with the half-sinusoidal current, leading to a theoretical 100% efficiency. In practice, harmonic control is usually conducted up to the third order, as further harmonic control yields limited efficiency improvement, but significantly increased implementation difficulty. Thus, the normalized voltage waveform of a Class-F PA with a finite number of harmonic terminations can be expressed as [7]

$$v_{\mathrm{F}}(\theta) = 1 - \frac{2}{\sqrt{3}}\cos\theta + \frac{1}{3\sqrt{3}}\cos 3\theta. \tag{3}$$

The above equation is able to deliver a 90.7% efficiency at the maximum power level. The voltage and current waveforms of the standard Class-F PA mode are plotted in Fig. 2(a), indicated by the red (in online version) (voltage) and black (current) curves.

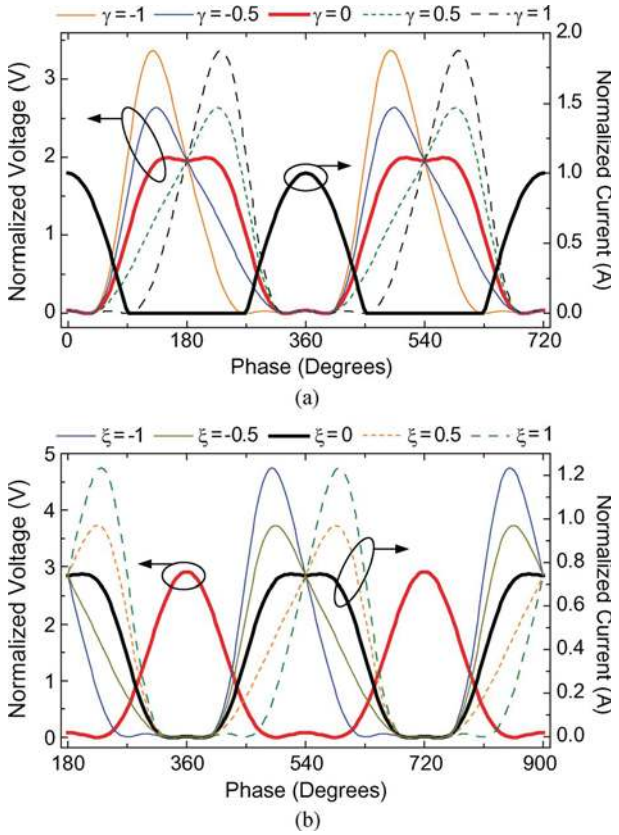

Fig. 2. Theoretical voltage and current waveforms. (a) Continuous Class-F for $-1 \le \gamma \le 1$ (0.1 of steps). (b) Continuous inverse Class-F for $-1 \le \xi \le 1$ (0.1 of steps).

Inverse Class-F PA mode is the dual of Class-F mode. It exploits dual harmonic loading conditions with O.C. even-harmonic loads and S.C. odd-harmonic loads, as shown in Fig. 1. This forms a square-wave current and half-sinusoidal-wave voltage, which can also lead to a theoretical 100% efficiency. In the practical case of controlling three harmonics, the voltage waveform is shaped by second-harmonic peaking [12]

$$v_{\mathrm{F}^{-1}}(\vartheta) = 1 + \frac{2}{\sqrt{2}}\cos\vartheta + \frac{1}{2}\cos 2\vartheta \tag{4}$$

while the current waveform takes the form of

$$i_{\mathrm{F}^{-1}}(\vartheta) = i_{\mathrm{DC}} - i_1\cos\vartheta + i_3\cos 3\vartheta \tag{5}$$

where $i_{\mathrm{DC}} = 0.37$, $i_1 = 0.43$, and $i_3 = 0.06$ [11]. The voltage and current waveforms of the standard inverse Class-F PA are plotted in red (in online version) and black, respectively, in Fig. 2(b).

B. Continuous Class-F/F^{-1} PA Modes

Recent investigations into continuous PA modes have demonstrated that the constant O.C. and S.C. conditions are not a unique solution for achieving optimal efficiency and output power. For the continuous Class-F mode, the voltage waveform

in (3) can be extended by multiplying a defining term, given by [10]

$$v_{\mathrm{CF}}(\theta) = \left(1 - \frac{2}{\sqrt{3}}\cos\theta + \frac{1}{3\sqrt{3}}\cos 3\theta\right) \times (1 - \gamma \sin\theta). \quad (6)$$

The case $\gamma = 0$ corresponds to the standard Class-F mode. The range of possible γ values must result in an absolute positive value of the second bracket, and thus the value of $v_{\mathrm{CF}}(\theta)$ in (6), as zero-crossing or negative voltage causes interaction with the knee region, and thus reduced efficiency [10]. Therefore, γ may vary from -1 to 1, leading to a family of voltage waveforms that offers a continuous design space with constant output performance, as shown in Fig. 2(a).

Similarly, the inverse Class-F (Class-F^{-1}) mode can also be extended to continuous Class-F^{-1} mode by modifying the current waveform as follows [12]:

$$i_{\mathrm{CF}^{-1}}(\vartheta) = (i_{\mathrm{DC}} - i_1 \cos\vartheta + i_3 \cos 3\vartheta) \times (1 - \xi \sin\vartheta). \quad (7)$$

Successful operation of this PA mode requires nonzero crossing current waveform, indicating a possible range of ξ from -1 to 1 [12]. Thus, a new family of current waveforms is formed, as plotted in Fig. 2(b). A standard Class-F^{-1} mode is formed when $\xi = 0$.

These continuous PA modes can be realized over the target bandwidth by applying the required harmonic impedances for the different γ or ξ values, which can be calculated using the following equation:

$$Z_n = -\frac{V_n}{I_n}. \quad (8)$$

where n represents the order of harmonic component. Here, we define R_{opt} as the optimum impedance of the standard Class-B mode with all harmonics short circuited, which is given by

$$R_{\mathrm{opt}} = \frac{V_{\mathrm{dc}} - V_{\mathrm{knee}}}{\frac{I_{\mathrm{peak}}}{2}}. \quad (9)$$

For the continuous Class-F mode, harmonic impedances are calculated using (2), (6), and (9) as follows:

$$\begin{aligned} Z_{\mathrm{F}} &= R_{\mathrm{opt}}\frac{2}{\sqrt{3}} + jR_{\mathrm{opt}}\gamma \\ Z_{2,\mathrm{F}} &= -jR_{\mathrm{opt}}\frac{7\sqrt{3}\pi}{24}\gamma \\ Z_{3,\mathrm{F}} &= \infty. \end{aligned} \quad (10)$$

The calculated harmonic loads of continuous Class-F mode with $-1 \le \gamma \le 1$ are plotted in the Smith charts shown in Fig. 3(a). The harmonic loads of continuous inverse Class-F PAs are obtained in a similar manner by substituting (4) and (7) into (9), which can be expressed in the admittance format as

$$\begin{aligned} Y_{\mathrm{F}^{-1}} &= G_{\mathrm{opt}}\sqrt{2}i_1 + jG_{\mathrm{opt}}\sqrt{2}i_{\mathrm{DC}}\xi \\ Y_{2,\mathrm{F}^{-1}} &= -jG_{\mathrm{opt}}2(i_1 + i_3)\xi \\ Y_{3,\mathrm{F}^{-1}} &= \infty. \end{aligned} \quad (11)$$

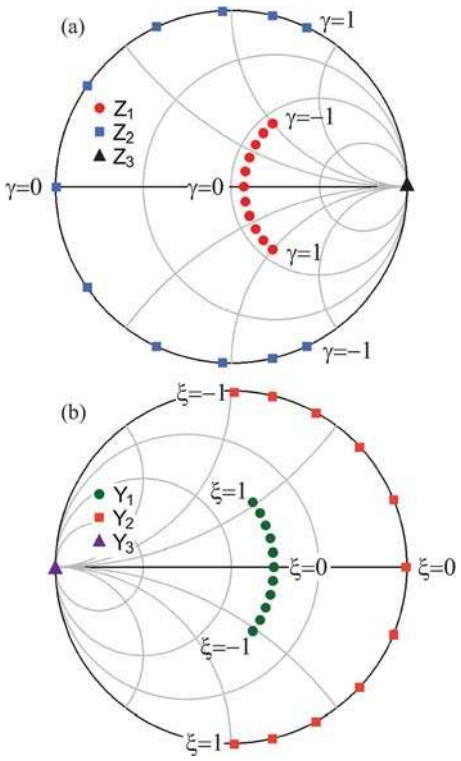

Fig. 3. Calculated first three harmonic loads. (a) Continuous Class-F in the impedance chart ($Z_0 = R_{\mathrm{opt}}$). (b) Continuous inverse Class-F in the admittance chart ($Y_0 = G_{\mathrm{opt}}$).

where $G_{\mathrm{opt}} = 1/R_{\mathrm{opt}}$. The calculated harmonic loads of continuous Class-F^{-1} mode are shown in Fig. 3(b) with $-1 \le \xi \le 1$.

A broadband PA with single continuous Class-F or F^{-1} mode faces two major challenges. First, it is difficult to fit the MN's impedance frequency response to the needed variation of the target loads with respect to γ or ξ. Second, it is practically very difficult to have the third harmonic located at a constant point as it is ideally desired, i.e., O.C. for continuous Class-F or S.C. for continuous Class-F^{-1}. However, it is noted from Fig. 3(a) and (b) that a combined utilization of these two continuous PA modes actually yields a further expanded design space. Also, by properly selecting the partial ranges of γ and ξ, it can be easier to fit the target loads to the MN behavior.

III. Broadband Harmonic-Tuned PA Design Using Mode Transferring

A. Realization of Mode Transferring Using Multistage Low-Pass MN

A proper MN is the key enabler for realizing broadband PAs. Recently, multistage low-pass topologies implemented using transmission lines (TLs) have been utilized for designing broadband high-efficiency PAs [3], [15], [22]. Design of such a complicated network requires network synthesis, which can be conducted using a real-frequency method [15], [22], [23] or methods based on low-pass filter prototypes [3]. Fig. 4(a) shows

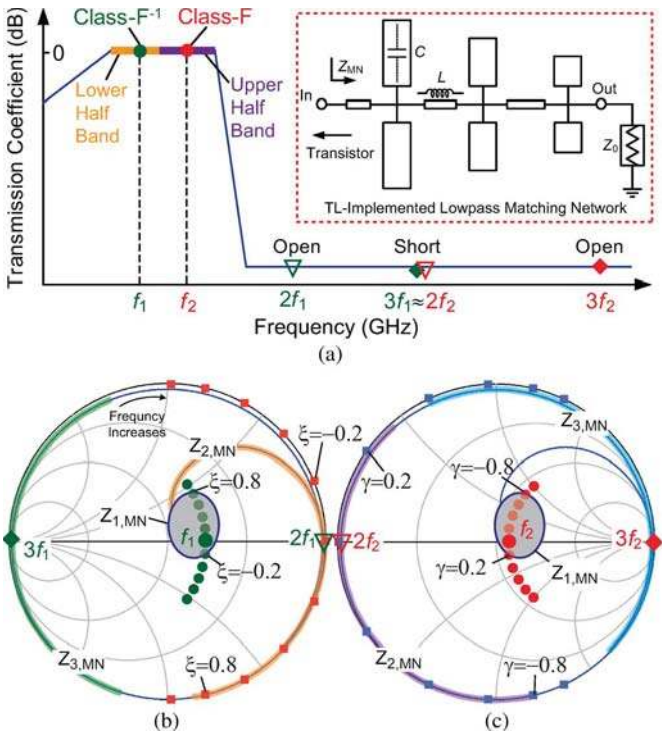

Fig. 4. Matching scheme. (a) Multistage TL-implemented low-pass MN and its frequency response. (b) Matching over the lower half band (continuous Class-F^{-1} mode). (c) Matching over the upper half band (continuous Class-F mode). ${}^{*}Z_{n,\mathrm{MN}}$ indicates the MN impedance at the nth harmonic frequencies.

a typical three-stage low-pass filter MN and its illustrative frequency response. In this network, inductors are implemented by high-impedance TLs and capacitors by low-impedance O.C. stubs (STs). As shown in Fig. 4(b) and (c), a well-synthesized low-pass matching filter can provide the fundamental matching over the desired bandwidth (octave band in this research), corresponding to the filter passband. The harmonic frequencies fall in the stopband of this low-pass filter while harmonic impedances are located at the edge of Smith chart as the stopband ideally yields a reflection coefficient of $\Gamma = 1$.

It is important to highlight that fitting the MN behavior to the target impedances of the continuous Class-F and F^{-1} modes does not require the entire ranges of γ and ξ. In particular, $-0.8 \leq \gamma \leq 0.2$ and $-0.2 \leq \xi \leq 0.8$ are preferable for performing the fundamental impedance matching using this low-pass topology, indicated in Fig. 4(b) and (c). As for the specific stopband impedance trajectory of this network, the continuous F^{-1} mode and continuous Class-F mode are expected to be realized across the lower and upper half parts of the entire band, respectively.

For the lower half band, the second harmonic impedance of the MN [$Z_{2,\mathrm{MN}}$, yellow highlighted (in online version)] tracks the target second harmonic impedance of continuous Class-F^{-1} mode ($Z_{2,\mathrm{F}^{-1}}$), as shown in Fig. 4(b). Meanwhile, the third harmonic impedance [$Z_{3,\mathrm{MN}}$, green highlighted (in online version)] of this band is located in the area indicated in Fig. 4(b), covering the S.C. point. Therefore, an exact continuous inverse Class-F mode can be realized at a frequency f_1 within the lower half band which has an S.C. $Z_{3,\mathrm{MN}}$. As the frequency increases to the upper half band, $Z_{2,\mathrm{MN}}$, highlighted in purple (in online version) in Fig. 4(c), moves clockwise and fits the target second harmonic impedance of continuous Class-F mode ($Z_{2,\mathrm{F}}$), while $Z_{3,\mathrm{MN}}$ covers the blue-highlighted (in online version) region. Thus, an optimized continuous Class-F mode is realized at f_2 within the upper half band, whose third harmonic impedance is located at the O.C. point. For the rest of the band other than f_1 and f_2, both the fundamental and second harmonics are both properly terminated, while the third harmonic is located along the edge of Smith chart, so a high efficiency can be still maintained [10].

Our previous design in [19] can be considered as a special case of this mode transferring between the continuous Class-F^{-1}/F modes. Fig. 4(a) underlines that f_1 and f_2 are almost located at around the middle points of the lower and upper half bands, respectively. Thus, they approximately follow the dependence of $f_1 \approx 2/3 f_2$. Also, $Z_{2f_1,\mathrm{MN}}$ can be very close to the O.C. point, as implied in Fig. 4(a) and (b). Therefore, a standard inverse Class-F PA is formed at f_1 and a standard Class-F PA at f_2, as is the case of [19]. With the combined utilization of continuous PA modes, the design space is greatly enlarged, while the target $Z_{2,\mathrm{F}^{-1}}$ and $Z_{2,\mathrm{F}}$ can be automatically distributed to the MN's stopband, as indicated in Fig. 4(b) and (c). Thus, in this design, the priority will be given to the fundamental impedance matching.

B. Transistor Modeling and Characterization

The initial target frequency range is an octave band from 1.5 to 3 GHz. Therefore, a dc–6-GHz 10-W Cree GaN transistor (CGH40010F) is used as the active device to experimentally demonstrate this design concept. As the theoretical PA mode analysis refers to the intrinsic drain plane (I-generation plane), the parasitics of the transistor need to be carefully modeled. This device consists of a CGH60015D bare chip and package. Thus, the computer-aided design (CAD)-based modeling can be conducted with a combination of the bare-chip model and the package model, which are provided by the manufacturer [24]. Compared to the packaged-transistor model, this combined model makes it easier to set up harmonic conditions in the load–pull characterization. The typical equivalent-circuit model of this transistor is shown in Fig. 5(a), indicating the intrinsic and package parasitics.

In this design, f_1 and f_2 are set to around the center points of the upper and lower half bands, respectively, given by $f_1 = 1.8$ GHz and $f_2 = 2.7$ GHz. First, the desired fundamental impedances for inverse Class-F and Class-F modes are extracted from load–pull simulations using Agilent Advanced Design System (ADS) [25]. The simulated impedances at the intrinsic drain plane are purely resistive, as plotted in Fig. 5(b), which represent the real parts of Z_{F} and $Z_{\mathrm{F}^{-1}} (= 1/Y_{\mathrm{F}^{-1}})$ in (10) and (11). Such impedances are transferred from the intrinsic-drain plane to the package plane at f_1 and f_2, respectively, shown in Fig. 5(b), yielding a reference for the output MN design. Subsequently, the simulated impedances are further extended to the continuous Class-F^{-1} and Class-F modes using (10) and (11), as shown in Fig. 5(c).

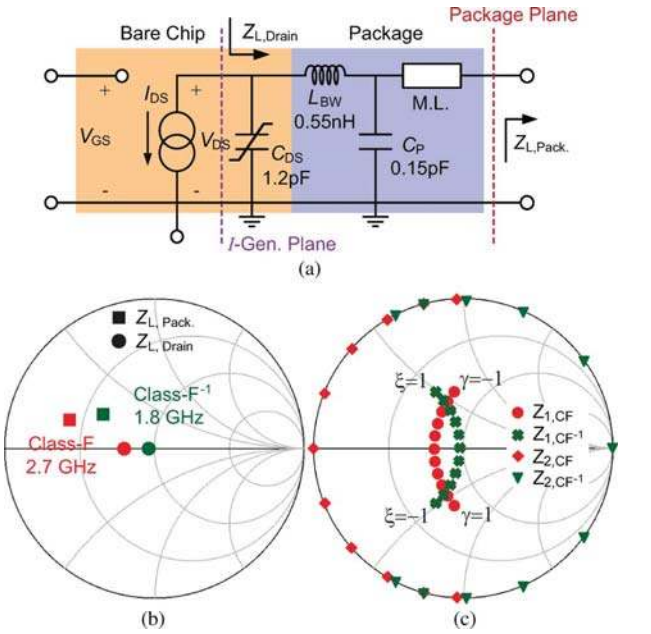

Fig. 5. Transistor modeling and characterization. (a) Equivalent-circuit model of CGH40010 showing the parasitics. (b) Simulated impedances at $f_1 = 1.8$ GHz and $f_2 = 2.7$ GHz. (c) Extended impedance ranges of continuous Class-F/F^{-1} modes.

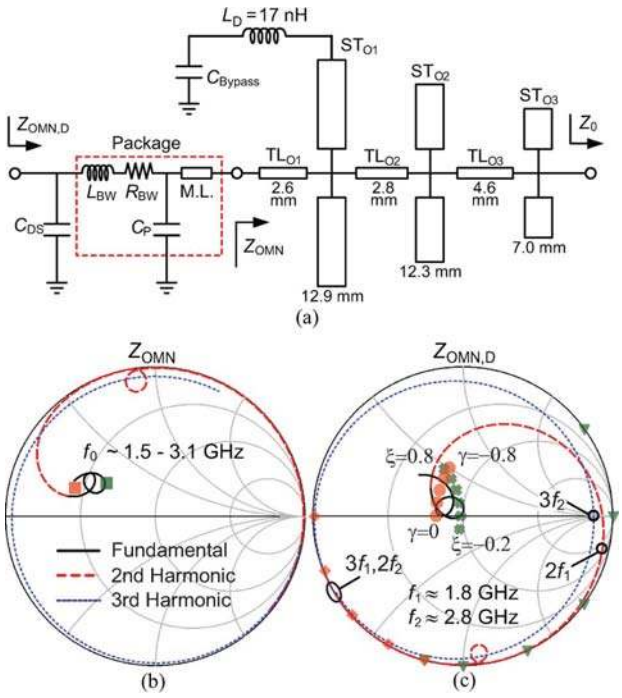

Fig. 6. Output MN design. (a) Circuit topology, (b) MN impedance. (c) Achieved impedance at intrinsic drain plane.

C. Output MN Design

The design and implementation of the low-pass MN have been studied in detail in [3]. This design follows a similar procedure, which mainly takes three steps.

Step 1) *Ideal-Network Synthesis*: A three-stage low-pass prototype is extracted from [26], which forms an octave-bandwidth impedance transformer with 4:1 transformation ratio. The prototype is then scaled to the desired frequency and 50-Ω reference impedance. Further, the real-to-real impedance transformer is transformed to a real-to-complex one referred to the extracted $Z_{\mathrm{L,Pack.}}$ in Fig. 5(b) using an ADS optimizer.

Step 2) *Implementation Using TLs*: The synthesized ideal network is implemented using TLs. In this design, the inductors are realized by high-impedance TLs, while the capacitors are replaced by low-impedance O.C. STs. For implementation on a Rogers 5880 PCB substrate,[1] the width of TLs and STs are 20 and 90 mil, respectively, considering the fabrication tolerance and dispersive effect. The corresponding TL and ST impedances are 95 and 36 Ω, respectively.

Step 3) *Post Optimization*: To realize the desired transferring PA mode, the implemented OMN is connected to the parasitic model of the transistor to obtain the impedance at the intrinsic-drain plane, as shown in Fig. 6(a). This means that the parasitic network now becomes a part of the OMN. The length of each TL section is finely tuned to properly align the OMN impedance trajectory to the target impedances at both the fundamental and harmonic frequencies. The tuned OMN is finally optimized together with the actual transistor model to achieve maximum efficiency. The finalized lengths of TLs and STs are indicated in Fig. 6(a).

Fig. 6(b) and (c) shows the fundamental, second-, and third-harmonic impedances at the package plane (Z_{OMN}) and intrinsic-drain plane $(Z_{\mathrm{OMN,D}})$, respectively. It can be seen in Fig. 6(b) that the implemented OMN yields the desired fundamental matching over the target bandwidth since the impedance is very close to the optimal points at f_1 and f_2. At the intrinsic drain plane, as shown in Fig. 6(c), the fundamental impedance, provided by the OMN, fits well with the target $Z_{\mathrm{F}^{-1}}$ and Z_{F} with $-0.2 < \xi < 0.8$ and $-0.8 < \gamma < 0$, respectively. The second harmonic impedance also tracks well with the target $Z_{2,\mathrm{F}^{-1}}$ and $Z_{2,\mathrm{F}}$ with the same ranges of γ and ξ. The third harmonic impedance moves across the O.C. and S.C. points as expected. Specifically, an exact continuous Class-F^{-1} mode is realized at $f_1 \approx 1.8$ GHz, while an optimal continuous Class-F mode is realized at $f_2 \approx 2.8$ GHz (slightly higher than the initial value). The impedance at $3f_1 (\approx 2f_2)$ is designed to be slightly capacitive $(\approx 0 + 10j)$ as it leads to a higher efficiency than the pure-zero impedance [27]. This could be due to the nonlinear behavior of C_{DS}.

IV. PA Implementation

A. PA Design and Fabrication

In [19], the input MN is implemented with a multisection TL transformer. In this study, the input MN is redesigned with a low-pass topology, which is less area consuming. A four-stage low-pass prototype is extracted from [26], as the input matching

[1]Rogers Corporation, Rogers, CT. [Online]. Available: http://www.rogerscorp.com/

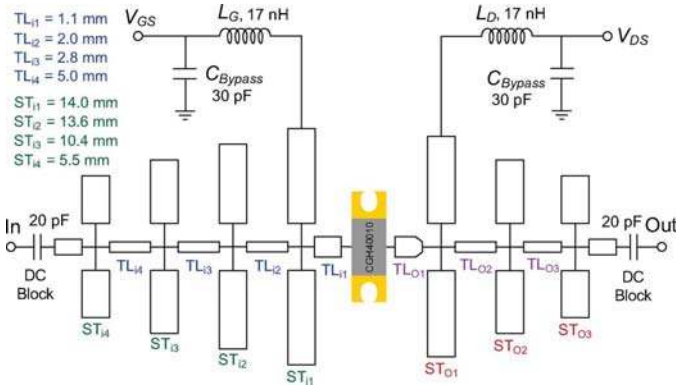

Fig. 7. Circuit schematic of the broadband harmonic-tuned PA.

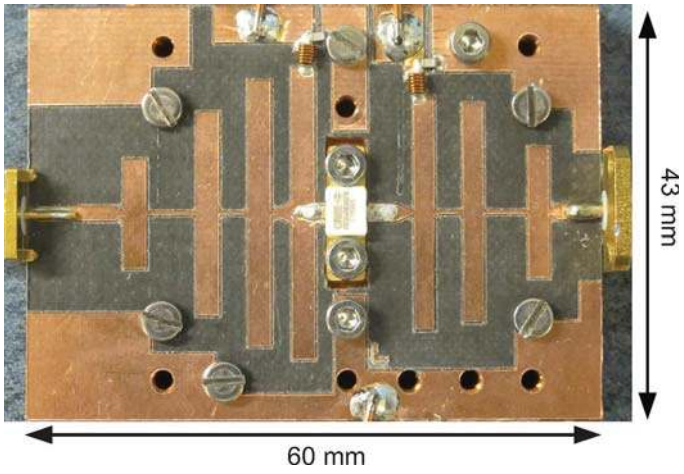

Fig. 8. Fabricated PA circuit.

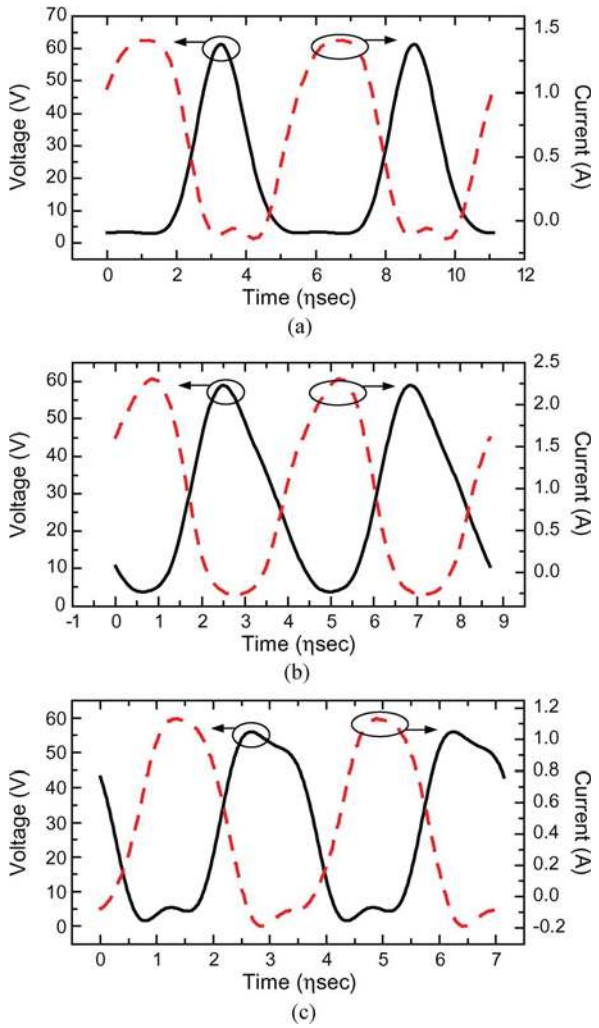

Fig. 9. De-embedded intrinsic drain waveforms of voltage and current from ADS simulation. (a) At 1.8 GHz (standard inverse Class-F). (b) At 2.3 GHz (continuous inverse Class-F). (c) At 2.8 GHz (continuous Class-F).

requires a larger impedance transformation ratio than the output one. This network is then implemented with TLs, the same as the ones in the output network. The schematic is shown in Fig. 7, indicating the input circuit topology and parameters of each TL sections.

The entire PA is implemented by connecting the transistor to the designed input and output MNs, as illustrated in Fig. 7. Here, the geometric dimensions of $\mathrm{TL_{i1}}$ and $\mathrm{TL_{o1}}$ are slightly adjusted to fit the package pads of the transistor, while maintaining the MNs' performance. The biasing networks are realized by a 17-nH inductor and 30-pF bypass capacitor. The PA is fabricated on a Rogers 5880 substrate and is mounted on a copper fixture, as shown in Fig. 8. The footprint of the fabricated PA is 60×43 mm^2. Compared to the previous design in [19], this design has a more compact circuit with a size reduction of larger than 30%, which is mainly due to the redesigned input MN.

B. Waveform Engineering

The entire PA model is established in ADS and simulated using the harmonic-balance simulator. Fig. 9(a)–(c) shows the simulated voltage and current waveforms at the intrinsic drain plane, when the broadband PA is operating at 1.8, 2.3, and 2.8 GHz with 10-W output power. Fig. 9(a) depicts a standard inverse Class-F PA waveform with half-sinusoidal voltage and quasi-square-wave current, which is basically due to the specific harmonic conditions applied at this frequency. A continuous Class-F^{-1} waveform is observed at 2.3 GHz, as shown in Fig. 9(b). Compared to the ideal waveform shown in Fig. 2(b), this waveform corresponds approximately to $\xi = -0.8$. A continuous Class-F waveform is obtained at 2.8 GHz, as shown in Fig. 9(c). This waveform corresponds to the case of a slightly negative γ, as indicated by the ideal waveforms in Fig. 2(a). This is the result of the harmonic condition applied at f_2 [see Fig. 6(c)].

V. Experimental Results

A. Continuous-Wave (CW) Evaluation

The PA is first tested under the stimulus of a single-tone CW signal swept from 1.3 to 3.3 GHz with 0.1-GHz step. The transistor gate is biased at the threshold of -3.3 V. The drain bias voltage is set to the value that leads to the optimal power-added efficiency (PAE) in the testing, which varies at different frequencies, as shown in Fig. 10. The CW signal is generated by an Agilent E4433B signal generator and boosted by a commercial

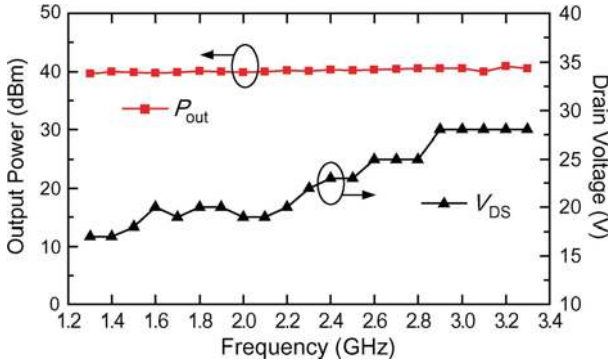

Fig. 10. Measured output power and the optimal drain bias point across the entire bandwidth.

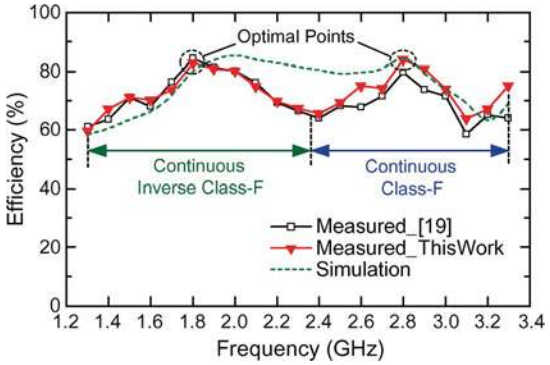

Fig. 11. Simulated and measured efficiency over the entire bandwidth.

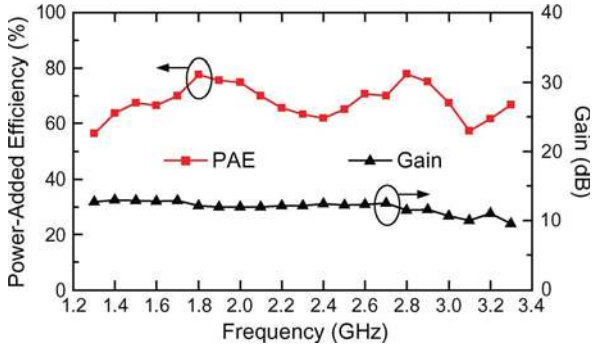

Fig. 12. Measured PAE and gain across the entire frequency range.

TABLE I
STATE-OF-THE-ART BROADBAND HIGH-EFFICIENCY PAs

Ref.	Class	BW (GHz, %)	P_{out}(W)	DE(%)	AE(%)	FE*
[3]	E	0.9–2.2, 84	10–20	63–89	76.5	85.3
[8]	J	1.4–2.6, 60	9–11	60–70	65.0	77.2
[15]	CF	1.45–2.45, 51	11–17	70–81	75.5	89.2
[16]	CF	0.55–1.1, 66	8–13	55–80	74.0	70.5
[30]†	N/A	1.9–4.3, 78	10–15	57–72	65.0	86.2
This Work	CF^{-1} /CF	1.3–3.3, 87	10–11	60–83	72.7	89.5

CF: continuous Class-F, CF^{-1}: continuous inverse Class-F, DE: drain efficiency, AE: average efficiency.

$*$ FE denotes the frequency-weighted efficiency, $AE/(\%) \times$ center frequency$/(\mathrm{GHz})^{0.25}$, similar to the metric used in MTT-5 Student PA Design Competition.

† The design is based on a bare-chip transistor.

driver amplifier (Mini-Circuits, ZHL-16W-43+)[2] to provide a sufficient input power of up to 30 dBm for the broadband testing. The PA output power is measured using an Agilent E4448 spectrum analyzer. Fig. 10 shows the measured fundamental output power from 1.3 to 3.3 GHz, which is around 10 W across the entire frequency band.

Fig. 11 shows the measured and simulated efficiency within the entire frequency range. The efficiency curve has two local maxima at $f_1 = 1.8$ GHz and $f_2 = 2.8$ GHz with $\geq$80% values, corresponding to the optimal continuous inverse Class-F and Class-F modes (second and third harmonics conditions are both satisfied), respectively. The overall measured efficiency is from 60% to 84% with an average value of around 73%. Simulation agrees well with the measurement for the majority of the band, while a small difference occurs around the frequency point of mode transition (see Fig. 11). This is mainly due to inaccuracies in the modeling and fabrication. To extract the PAE, the power gain of the PA is considered and measured, which ranges from 10 to 13 dB within the entire bandwidth, as shown in Fig. 12. A PAE of 56% to 79% is measured.

This design exhibits a state-of-the-art PA performance compared to the contemporary broadband PA results recently published, listed in Table I. A frequency-weighted average efficiency (FE) is introduced here to evaluate the PA efficiency together with frequency, which has often been utilized in the MTT-5 Student Design Competition and [14]. It can be seen from Table I that this paper, in particular, presents the widest fractional bandwidth and the highest frequency-weighted efficiency. We attribute this excellent performance to the combined utilization of two continuous PA modes, while other studies are all based on a single mode.

The PA is also characterized under different driving powers to evaluate its dynamic performance. Fig. 13(a) and (b) shows the measured gain, drain efficiency, and PAE versus input power at 1.8 and 2.8 GHz, respectively. The gain compresses at $P_{in} = 22$ dBm and $P_{in} = 28$ dBm for these two frequencies, corresponding to the maximum PAE values. It is also seen from Figs. 13 that >50% efficiency can be maintained within 5 dB of output power back-off, indicating a good potential for amplifying amplitude-modulated signals.

B. Modulated Evaluation

To evaluate the PA performance in an actual communication system, the implemented PA is tested with a 16 quadrature-amplitude-modulation (16QAM) signal with a symbol rate of 300 ks/s, which has peak-to-average power ratio of around 7 dB. This 16QAM signal is generated by an Agilent E4438C signal generator and is amplified to a sufficient driving level by the commercial PA used in Section V-A. The biasing condition used in this measurement is also the same as that in the CW evaluation. The measured PA performance over the entire frequency band is shown in Fig. 14, indicating an average output power of around 36 dBm, average gain of around 10 dB, and average efficiency of 30%–48%. These curves have similar shapes with the corresponding CW results, as shown in Section V-A.

[2]Mini-Circuits Corporation, Brooklyn, NY. [Online]. Available: http://www.minicircuits.com/

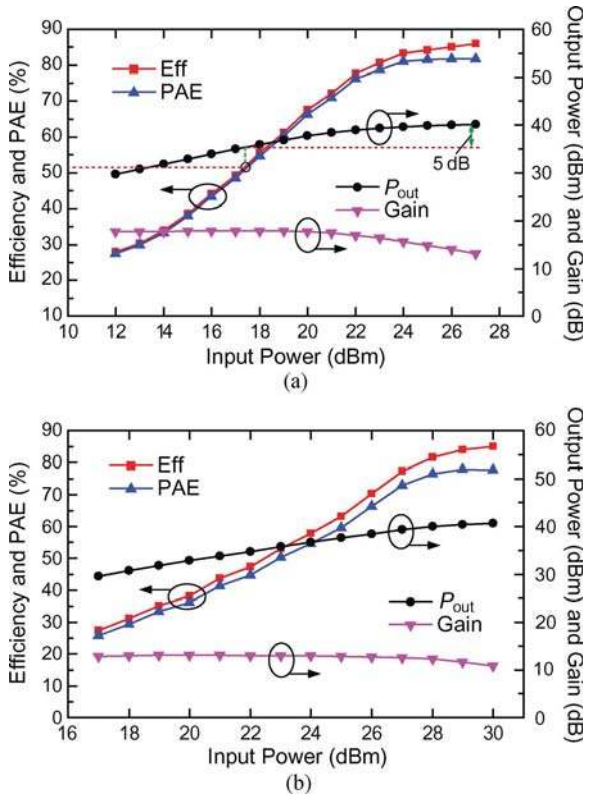

Fig. 13. Measured PA performance versus input power at: (a) 1.8 and (b) 2.8 GHz.

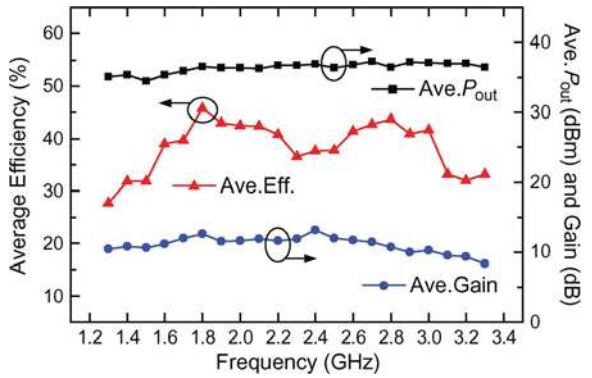

Fig. 14. Measured broadband PA performance characterized under stimulus of a frequency-swept 16QAM signal.

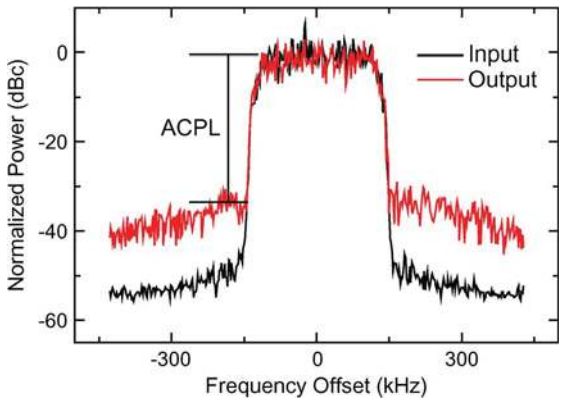

Fig. 15. Measured output spectrum under stimulus of a 300-kHz 16QAM signal at 2.8 GHz.

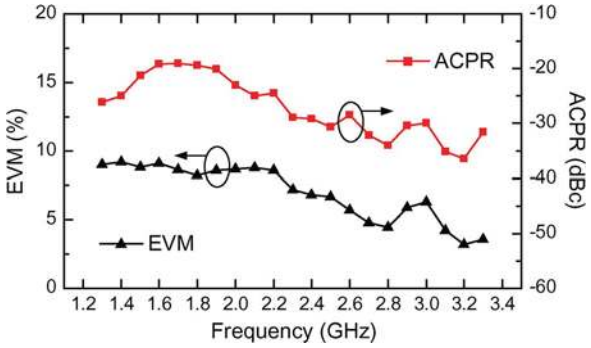

Fig. 16. Measured EVM and ACPR over the entire bandwidth.

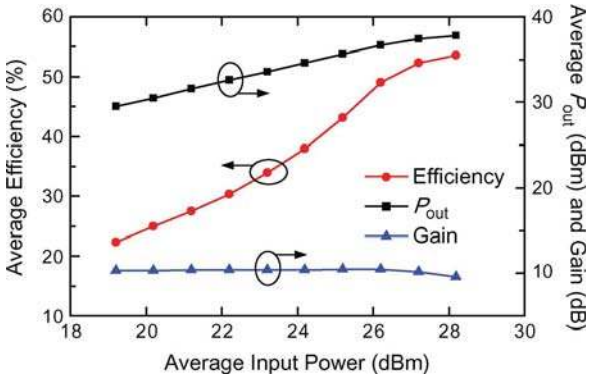

Fig. 17. Measured PA performance with a power-swept input stimulus.

Fig. 15 plots the measured output spectrum at 2.8 GHz with an average input power of 25 dBm, exhibiting an adjacent channel power ratio (ACPR) of 32 dBc measured at 150-kHz frequency offset. Compared to the input spectrum, the spectrum regrowth only leads to an ACPR increase of 13 dB at this frequency, indicating a good linearity performance of this PA. The system-level linearity performance of this PA is measured using a real-time spectrum analyzer (Tektronix RSA3408A). Fig. 16 presents the measured error vector magnitude (EVM) and ACPR across the desired bandwidth, showing an overall EVM of 3%–9% and ACPR from -36 to -20 dBc. Improved linearity is observed for the upper half band, which could be due to the mitigation of transistor's switching behavior at higher frequencies.

Subsequently, the PA is tested with a power-swept QAM signal (from 19 to 28 dBm). Fig. 17 shows the measured average output power, gain, and efficiency with respect to the input power. The gain compression point is around 26 dBm of input power, while the maximum efficiency of 50% is achieved at input power of 28 dBm. Fig. 18 shows the linearity performance of the PA versus input power. The EVM and ACPR are at very low levels for small $P_{\rm in}$ (EVM $<$4.2%, ACPR < -33 dBm), and they increase sharply with input power when $P_{\rm in} \geq 24$ dBm. It can be seen from Figs. 17 and 18 that optimal input power is around 25 dBm for a QAM signal that yields a good balance between efficiency and linearity.

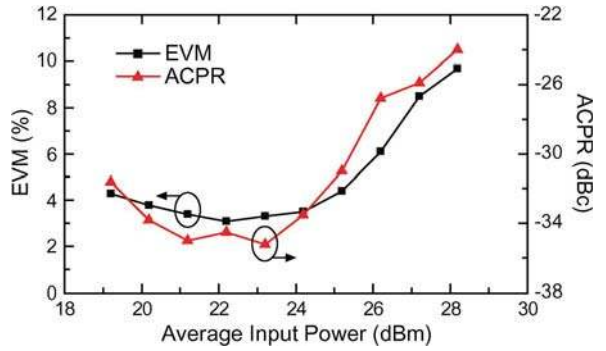

Fig. 18. Measured EVM and ACPR versus input power.

VI. Conclusion

This paper has presented an innovative approach for designing high-frequency broadband harmonic-tuned PAs based on mode-transferring between continuous inverse Class-F and continuous Class-F. Compared to the single continuous Class-F/F^{-1} mode, such a hybrid PA mode can be easier to realize over an octave bandwidth. Specifically, the target fundamental and harmonic impedances can be well fitted to the frequency behavior of a three-stage low-pass MN implemented using TLs. For technology demonstration, a broadband PA was designed exploiting this method with a commercial 10-W GaN transistor. The in-band PA-mode transferring between continuous Class-F^{-1} and continuous Class-F is demonstrated using waveform engineering. The fabricated PA exhibits an overall bandwidth of from 1.3 to 3.3 GHz (87% fractional bandwidth) with state-of-the-art measured performance, i.e., drain efficiency of 60%–84%, gain of $>$10-dB, and output power of 10 W. Moreover, modulated evaluation with a 300-kHz bandwidth 16-QAM signal reveals a good linearity performance of this PA with ACPR from -20 to -35 dBc and EVM of 4%–9% throughout the entire bandwidth.

Acknowledgment

The authors would like to thank Cree Inc., Durham, NC, for supplying the large-signal transistor models and application documents.

References

[1] M. P. van der Heijden, M. Acar, and J. S. Vromans, "A compact 12-watt high-efficiency 2.1–2.7 GHz class-E GaN HEMT power amplifier for base stations," in *IEEE MTT-S Int. Microw. Symp. Dig.*, Jun. 2009, pp. 657–660.

[2] A. A. Tanany, A. Sayed, and G. Boeck, "Broadband GaN switch mode class E power amplifier for UHF applications," in *IEEE MTT-S Int. Microw. Symp. Dig.*, Jun. 2009, pp. 761–764.

[3] K. Chen and D. Peroulis, "Design of highly efficient broadband class-E power amplifier using synthesized low-pass matching networks," *IEEE Trans. Microw. Theory Techn.*, vol. 59, no. 12, pp. 3162–3173, Dec. 2011.

[4] T. B. Mader, E. W. Bryerton, M. Markovic, M. Forman, and Z. Popovic, "Switched-mode high-efficiency microwave power amplifiers in a free-space power-combiner array," *IEEE Trans. Microw. Theory Techn.*, vol. 46, no. 10, pp. 1391–1398, Oct. 1998.

[5] E. Cipriani, P. Colantonio, F. Giannini, and R. Giofre, "Optimization of class E power amplifier design above theoretical maximum frequency," in *Proc. Eur. Microw. Integr. Circuits Conf.*, Oct. 2008, pp. 514–517.

[6] S. Jee, J. Moon, J. Kim, J. Son, and B. Kim, "Switching behavior of class-E power amplifier and its operation above maximum frequency," *IEEE Trans. Microw. Theory Techn.*, vol. 60, no. 1, pp. 89–98, Jan. 2012.

[7] S. C. Cripps, *RF Power Amplifier for Wireless Communications*, 2nd ed. Boston, MA: Artech House, 2006.

[8] P. Wright, J. Lees, J. Benedikt, P. J. Tasker, and S. C. Cripps, "A methodology for realizing high efficiency class-J in a linear and broadband PA," *IEEE Trans. Microw. Theory Techn.*, vol. 57, no. 12, pp. 3196–3204, Dec. 2009.

[9] V. Carrubba, A. L. Clarke, M. Akmal, J. Lees, J. Benedikt, P. J. Tasker, and S. C. Cripps, "The continuous class-F mode power amplifier," in *40th Eur. Microw. Conf.*, Oct. 2010, pp. 1675–1677.

[10] V. Carrubba, A. L. Clarke, M. Akmal, J. Lees, J. Benedikt, P. J. Tasker, and S. C. Cripps, "On the extension of the continuous class-F mode power amplifier," *IEEE Trans. Microw. Theory Techn.*, vol. 59, no. 5, pp. 1294–1303, May 2011.

[11] V. Carrubba, A. L. Clarke, M. Akmal, J. Lees, J. Benedikt, S. C. Cripps, and P. J. Tasker, "Exploring the design space for broadband pas using the novel "continuous inverse class-F mode"," in *41st Eur. Microw. Conf.*, Oct. 2011, pp. 333–336.

[12] V. Carrubba, A. L. Clarke, M. Akmal, J. Lees, J. Benedikt, S. C. Cripps, and P. J. Tasker, "The continuous inverse class-F mode power amplifier with resistive second-harmonic impedance," *IEEE Trans. Microw. Theory Techn.*, vol. 60, no. 6, pp. 1928–1936, Jun. 2012.

[13] J. Moon, J. Kim, and B. Kim, "Investigation of class-J power amplifier with a nonlinear C_{out} for optimized operation," *IEEE Trans. Microw. Theory Techn.*, vol. 58, no. 11, pp. 2800–2811, Nov. 2010.

[14] J. Kim, J. Kim, J. Moon, J. Son, I. Kim, J. Jee, and B. Kim, "Saturated power amplifier optimized for efficiency using self-generated harmonic current and voltage," *IEEE Trans. Microw. Theory Techn.*, vol. 59, no. 8, pp. 2049–2058, Aug. 2011.

[15] N. Tuffy, L. Guan, A. Zhu, and T. J. Brazil, "A simplified broadband design methodology for linearized high-efficiency continuous class-F power amplifiers," *IEEE Trans. Microw. Theory Techn.*, vol. 60, no. 6, pp. 1952–1963, Jun. 2012.

[16] V. Carrubba, J. Lees, J. Benedikt, P. J. Tasker, and S. C. Cripps, "A novel highly efficient broadband continuous class-F RFPA delivering 74% average efficiency for an octave bandwidth," in *IEEE MTT-S Int. Microw. Symp. Dig.*, Jun. 2011, pp. 1–4.

[17] P. Saad, H. M. Nemati, M. Thorsell, K. Andersson, and C. Fager, "An inverse class-F GaN HEMT power amplifier with 78% PAE at 3.5 GHz," in *39rd Eur. Microw. Conf.*, Oct. 2009, vol. 1, pp. 496–499.

[18] K. Kuroda, R. Ishikawa, and K. Honjo, "Parasitic compensation design technique for a *C*-Band GaN HEMT class-F amplifier," *IEEE Trans. Microw. Theory Techn.*, vol. 58, no. 11, pp. 2741–2750, Nov. 2010.

[19] K. Chen and D. Peroulis, "Design of high-efficiency power amplifier using in-band class-F^{-1}/F mode-transferring technique," in *IEEE MTT-S Int. Microw. Symp. Dig.*, Jun. 2012, pp. 1–4.

[20] Y. Ding, Y. X. Guo, and F. L. Liu, "High-efficiency concurrent dual-band class-F and inverse class-F power amplifier," *IET Electron. Lett.*, vol. 47, no. 15, pp. 847–849, Jul. 2011.

[21] F. H. Raab, "Maximum efficiency and output of class-F power amplifier," *IEEE Trans. Microw. Theory Techn.*, vol. 59, no. 6, pp. 2001–2005, Jun. 2001.

[22] J. Moon, J. Son, J. Lee, and B. Kim, "A multimode/multiband envelope tracking transmitter with broadband saturated amplifier," *IEEE Trans. Microw. Theory Techn.*, vol. 59, no. 12, pp. 3463–3473, Dec. 2011.

[23] D. Wu, F. Mkadem, and S. Boumaiza, "Design of a broadband and highly efficient 45 W GaN power amplifier via simplified real frequency technique," in *IEEE MTT-S Int. Microw. Symp. Dig.*, Jun. 2010, pp. 1090–1093.

[24] R. Pengelly, B. Millon, D. Farrell, B. Pribble, and S. Wood, "Application of non-linear models in a range of challenging GaN HEMT power amplifier designs," presented at the IEEE MTT-S Int. Microw. Symp. Workshop, Jun. 2008.

[25] ADS. Agilent Technol. Inc., Santa Clara, CA, 2009. [Online]. Available: http://www.agilent.com

[26] G. L. Matthaei, "Tables of Chebyshev impedance-transformation networks of low-pass filter form," *Proc. IEEE*, vol. 52, no. 8, pp. 939–963, Aug. 1964.

[27] P. Wright, A. Sheikh, P. J. Tasker, and J. Benedikt, "Highly efficient operation modes in GaN power transistors delivering upwards of 81% efficiency and 12 W output power," in *IEEE MTT-S Int. Microw. Symp. Dig.*, Jun. 2008, pp. 1147–1150.

[28] P. Saad, C. Fager, H. Cao, H. Zirath, and K. Andersson, "Design of a highly efficient 2-4-GHz octave bandwidth GaN-HEMT power amplifier," *IEEE Trans. Microw. Theory Techn.*, vol. 58, no. 7, pp. 1677–1685, Jul. 2010.

Kenle Chen (S'10) received the Bachelor's degree in communication engineering from Xi'an Jiaotong University, Xi'an, Shaanxi, China, in 2005, the Master's degree in electronics and information engineering from Peking University, Beijing, China, in 2008, and is currently working toward the Ph.D. degree at Purdue University, West Lafayette, IN.

From 2007 to 2008, he was with the Institute of Micro Electronics, National Key Laboratory of Micro/Nano Fabrication, Peking University, where his research focused on RF microelectromechanical systems (MEMS) switches, tunable filters, and vacuum packaging. He is currently with the School of Electrical and Computer Engineering and the Birck Nanotechnology Center, Purdue University. His research interests include broadband highly efficient PA design methodologies, adaptive PAs and transmitters, integration of PAs and high-Q filters (co-design technique), and high-power failure mechanisms of microwave devices.

Mr. Chen was the recipient of the Second and Third Place Awards of the Student High Efficiency Power Amplifier Design Competition, IEEE Microwave Theory and Techniques Society (IEEE MTT-S) International Microwave Symposium (IMS) in 2012 and 2011, respectively. He was also a recipient of the 2012 IEEE MTT-S Graduate Research Fellowship.

Dimitrios Peroulis (S'99–M'04) received the Ph.D. degree in electrical engineering from The University of Michigan at Ann Arbor, in 2003.

Since August 2003, he has been with Purdue University, West Lafayette, IN. He leads the Adaptive Radio Electronics and Sensors (ARES) Team, which focuses on reconfigurable analog/RF electronics for adaptive communications, signal intelligence, and harsh-environment sensors. He has been a Principle Investigator (PI)/co-PI in over 40 projects funded by government agencies and industry in these areas. Since 2007, he has been a key contributor to the Defense Advanced Research Projects Agency (DARPA) analog spectral processors (ASPs) (Phases I–III) project, resulting in the first widely tunable (tuning range $>$ 3:1) pre-select radio filters with unprecedented quality factors ($Q > 1000$) and power handling ($>$10 W) for high-frequency applications (1–30 GHz). A wide variety of reconfigurable filters with simultaneously adaptable features including frequency, bandwidth, rejection level, filter order, and group delay have been demonstrated over the past four years. His group recently codeveloped a ground-breaking concept of field programmable filter arrays (FPFAs). Inspired by field-programmable gate arrays (FPGAs) in digital systems, FPFAs are based on a sea of coupled resonators and multiple ports in order to enable reutilization of the same adaptive resonators to support diverse needs for dissimilar systems. Arbitrary operational modes and multiple operational channels may be created and reconfigured at will. He has made significant advances in high-power high-efficiency PAs and RF CMOS integrated circuits (ICs) with high-efficiency antennas. In the areas of sensors, he has also demonstrated the first wireless battery-free high-temperature microelectromechanical systems (MEMS) sensors for health monitoring of sensitive bearings in aircraft engines. These sensors continuously monitor (RF identification (RFID) type) the true temperature of the bearing to over 300 °C or 550 °C (depending on the design) and wirelessly transmit it to a base station. These sensors are based on well-established silicon processing for low-cost high-yield manufacturing. They have demonstrated extremely robust operation for over 1B cycles and continuous loading for over three months without failure.

Prof. Peroulis was the corecipient, along with his team, of Third Place in the Student PA Design Competition, 2011 IEEE Microwave Theory and Techniques Society (IEEE MTT-S) International Microwave Symposium (IMS). In addition, a student design team at Purdue University, of which he was assistant team leader, was the recipient of the First Place Awards in Phases I and II of the 2007–2008 SRC/SIA IC Design Challenge by demonstrating high-efficiency chip-to-chip wireless links with U-band transceivers. Further advances led to bond-wire Yagi antenna arrays with efficiencies exceeding $>$80%.